Electronic Supplementary Information

Sustainable scale resistance on bioinspired synergistic microspine coating with collectible liquid barrier

Ruhua Zang, [ab] Yixuan Wang,[ab] Jingxin Meng,[*abc] Wei Chen,[ab] Bing Wang,[ab] Xuetao Xu,[ab] Xiao He,[ab] Hui Yang,[a] Kan Li,[b] and Shutao Wang[*ab]

[a]CAS Key Laboratory of Bio-inspired Materials and Interfacial Science, Technical Institute of Physics and Chemistry, Chinese Academy of Sciences, Beijing 100190, P. R. China

[b]University of Chinese Academy of Sciences (UCAS), Beijing 100049, P. R. China

[c]Binzhou Institute of Technology, Binzhou 256600, P. R. China

***Corresponding authors.** E-mail: mengjx628@mail.ipc.ac.cn; stwang@mail.ipc.ac.cn

Contents:

3. Supplementary Tables

4. Supplementary Movies

1. Supplementary Notes

1.1 Materials

Polydimethylsiloxane (PDMS, Sylgard 184) and silicone oil (10 cSt) were purchased from Dow Corning (USA). N-hexane (denoted as C6), n-decane (C10), n-dodecane (C12), n-hexadecane (C16), n-eicosane (C20), n-tetracosane (C24) and 1*H*, 1*H*, 2*H*, 2*H*-perfluorodecyltrimethoxysilane (FAS; AR) were purchased from J&K Scientific Ltd. (China). Calcium sulfate hemihydrate ($CaSO_4 \cdot 1/2H_2O$, 97%) was purchased from Acros Organics (Belgium). 1,1'-dioctadecyl-3,3,3',3'-tetramethylindocarbocyanine perchlorate (DiI) was purchased from Aladdin Chemical (China). Ethylenediamine tetraacetic acid disodium salt (EDTA-Na_2, AR) was purchased from Sinopharm Chemical Reagent Co., Ltd. (China). All aqueous solutions were prepared using deionized water (Milli-Q system, 18.2 MΩ·cm, Bedford, MA, USA). Commercial sewing needles were purchased at the Shuangyan Company (China). The sandpaper (300#) was obtained from Eagle Company (China). All reagents were used directly without further purification.

1.2 Characterization

Environmental scanning electron microscope (ESEM) and energy dispersive spectrometry (EDS) images were achieved by using an ESEM (FEI, Quanta FEG 250, USA). The microspine replica template was fabricated with a jet dispensing system (B-300S, Weisheng, China). The microscope image of the micro-sized oil droplets in the artificial oilfield produced water was observed by using an optical microscope (Ti-E, Nikon, Japan). The deposited scale (i.e., $CaSO_4$) was quantified by Inductively Coupled Plasma Atomic Emission Spectroscopy (ICP-AES, Varian 710-OES, USA). Static contact angles (CAs) were measured on a OCA20 contact angle system (Data-physics, Germany) at ambient temperature. Dynamic scale-resistant process and oil collection process on a single microspine were recorded by a charge-coupled device of the OCA20 system. Friction and adhesion measurements were performed on a conventional ball-on-disk reciprocating tribometer (Tribometer UMT-2, CETR, Bruker, USA). The movie of de-scaling process was obtained by a digital camera (Canon Power shot A1100IS).

1.3 The critical value of oil content for a stable oil layer

To explore the role of oil content in oil layer stability, we compare oil weight changes (ΔW) of the BLOCK coating before and after immersion in an oil/water mixture for 24 h (see main text, Fig. 3b). ΔW could be calculated from the formula: $\Delta W = (V_C - V_L) \times t$. V_C is oil collection rate, V_L is oil loss rate and t is immersing time.

Taking a flow rate of 6.1 mL/s for an example, V_L is a constant value from fluid flushing [1] under the fixed flow rate while V_C increases with the increase of oil content from 0 to 5%. For oil content <1.7% (e.g., 0.5% oil, v/v), ΔW decreases over time from $V_C < V_L$. By contrast, for oil content >1.7% (e.g., 2% oil), ΔW significantly increases with time at first and then approaches a plateau, which results from $V_C > V_L$. Therefore, we chose 1.7% oil content as the critical value for achieving a stable oil layer.

1.4 Mechanism of oil collection

To directionally collect oil droplets from a flowing oil/brine mixture, the oil droplet is driven by the sum of Laplace pressure (F_L) and hysteresis resistance force (F_H) in Fig. S14d.

From a gradient of geometric curvature on the conical microspine, the Laplace pressure can directionally move the oil droplet. F_L can be calculated as follows:[1]

$$F_L \sim (\gamma_w - \gamma_o)\left(\frac{1}{R_1} - \frac{1}{R_2}\right)\frac{\sin\alpha}{R_2 - R_1}V \tag{S1}$$

where γ_w and γ_o stand for the surface tension of water and oil, R_1 and R_2 denote the local radius of the microspine at the two opposite sides of the oil droplet, α is the apex angle of the microspine and V is the volume of the oil droplet.

From the capillary force, hysteresis resistance force opposes the movement of micro-sized oil droplet. F_H can be estimated as follows:[1]

$$F_H \sim \pi R_0(\gamma_w - \gamma_o)(\cos\theta_r - \cos\theta_a) \tag{S2}$$

where R_0 is the radius of the oil droplet, θ_r and θ_a are the receding and advancing contact angles of the oil droplet, respectively.

1.5 Spreading of the oil droplet on BLOCKs

The spreading of oil droplet on BLOCKs underwater can be evaluated by the oil spreading performance on the oil-infused PDMS substrate in a salt solution, which can be estimated by spreading coefficient (S) as follows:[2]

$$S_{os(w)} = \gamma_{sw} - (\gamma_{ow} + \gamma_{so}) \tag{S3}$$

where γ_{sw}, γ_{ow} and γ_{so} are interfacial tensions of substrate-salt solution, oil layer-salt solution and substrate-oil layer, respectively.

In water, the silicone oil wets the oil-infused PDMS substrate with a contact angle of ~0° ($S_{os(w)} > 0$,[3, 4] Fig. S15).

1.6 The calculation of contact angle of the crystal nucleus on the PDMS with/without oil

Based on the classical nucleation theory and Young's equation, the contact angle of the crystal nucleus on the substrate in a salt solution (θ_1) in Fig. S1 can be expressed as:[5, 6]

$$\cos\theta_1 = \frac{\gamma_{s2l1} - \gamma_{s1s2}}{\gamma_{s1l1}} \tag{S4}$$

where s_1, s_2, and l_1 represent crystal nucleus, substrate and salt solution. γ_{s1s2} and γ_{s1l1} are the interfacial energies of crystal nucleus-substrate and crystal nucleus-salt solution, respectively. The interface tension of substrate-salt solution (γ_{s2l1}) can be expressed as:

$$\gamma_{s2l1} = \gamma_{s2g} - \gamma_{l1g}\cos\theta_2 \tag{S5}$$

where g represents air. γ_{s2g} and γ_{l1g} are the interfacial energies of substrate-air and salt solution-air, respectively. θ_2 is the contact angle of a salt droplet on the substrate in air (Fig. S17a). The interface tension of crystal nucleus-substrate (γ_{s1s2}) can be estimated as:[7-9]

$$\gamma_{s1s2} = \gamma_{s1} + \gamma_{s2} - 2\sqrt{\gamma_{s1}\gamma_{s2}} \tag{S6}$$

where γ_{s1} and γ_{s2} are the surface energies of crystal nucleus and substrate, respectively.

By the combination of equations (S4) and (S5), $\cos\theta_{1(without\ oil)}$ can be obtained for the PDMS substrate generating a liquid/solid/solid scaling environment:

$$\cos\theta_{1(without\ oil)} = \frac{\gamma_{s2g} - \gamma_{l1g}\cos\theta_2 - \gamma_{s1s2}}{\gamma_{s1l1}} \tag{S7}$$

Furthermore, the PDMS substrate can be replaced by oil due to the existence of a stable oil layer for the oil-infused PDMS substrate, forming a liquid/solid/liquid scaling environment. Equation (S4) can be replaced by:

$$\cos\theta_{1(with\ oil)} = \frac{\gamma_{l2l1} - \gamma_{s1l2}}{\gamma_{s1l1}} \tag{S8}$$

where l_2 represents oil. γ_{l2l1} is the interfacial energy of oil-salt solution. The crystal nucleus-oil interface tension (γ_{s1l2}) can be expressed as:

$$\gamma_{s1l2} = \gamma_{s1l1} - \gamma_{l2l1}\cos\theta_3 \tag{S9}$$

where θ_3 is the contact angle of the oil droplet on crystal in a salt solution (Fig. S17b).

By combining equations (S8) and (S9) for the oil-infused PDMS substrate, $\cos\theta_{1(with\ oil)}$ can be obtained:

$$\cos\theta_{1(with\ oil)} = \frac{\gamma_{l2l1}}{\gamma_{s1l1}}(1 + \cos\theta_3) - 1 \tag{S10}$$

The related interfacial energies between different phases were summarized in Table S1. The contact angles of a salt droplet on the substrate in air (θ_2) and an oil droplet on crystal in salt

solution (θ_3) are ca. 110° and 165°, respectively. Hence, the corresponding $\cos\theta_{1(without\ oil)}$ and $\cos\theta_{1(with\ oil)}$ are ca. 0.37 and -0.99.

1.7 The calculation of scale crystal-substrate and scale crystal-salt solution interfacial energies

The interfacial energy between phase 1 and phase 2 can be calculated by utilizing the following equation:[9]

$$\gamma_{12} = \left(\sqrt{\gamma_1^{LW}} - \sqrt{\gamma_2^{LW}}\right)^2 + 2\left(\sqrt{\gamma_1^+\gamma_1^-} + \sqrt{\gamma_2^+\gamma_2^-} - \sqrt{\gamma_1^+\gamma_2^-} - \sqrt{\gamma_1^-\gamma_2^+}\right) \quad \text{(S11)}$$

where γ^+, γ^- and γ^{LW} denote the polar components from the Lewis acid and base sites and the nonpolar component of surface energy, respectively.

The surface tension components of gypsum crystal, salt solution and substrate (PDMS) were taken from literature [2, 10, 11] and summarized in table S2. The interfacial energies of scale crystal-substrate (γ_{s3s2}) and scale crystal-salt solution (γ_{s3l1}) are 12.7 and -21 mJ/m^2, respectively.

2. Supplementary Figures

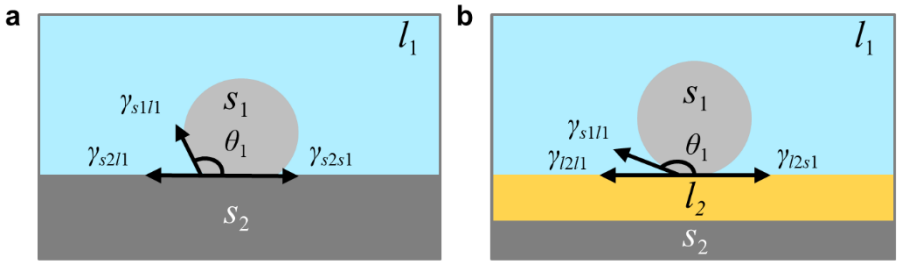

Fig. S1. Introducing oil layer changes the underwater scaling micro-environment from liquid/solid/solid to liquid/solid/liquid triphase systems. (a) Scale crystal nucleation on a smooth substrate in a salt solution presenting water/scale/substrate triphase system. (b) Scale crystal nucleation on the oil layer in a salt solution providing water/scale/oil triphase system. θ_1 is the contact angle of the crystal nucleus on the substrate. s_1 and s_2 represent scale crystal and the substrate. l_1, and l_2 are salt solution and oil, respectively.

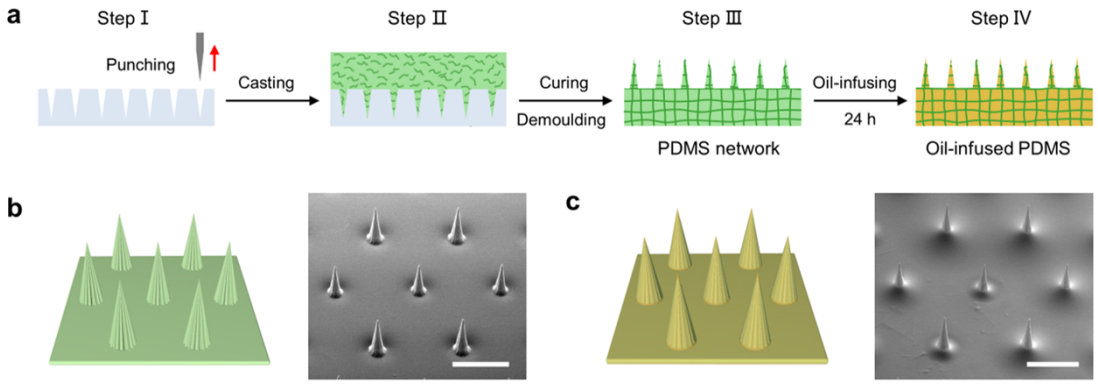

Fig. S2. Fabrication and characterization of BLOCKs. (a) Firstly, the PE template was prepared by punching the flat PE plate with a rough sewing needle from a jet dispensing system (Step I). Then, the PDMS precursor (a mixture of curing agent and silicone oligomer) was casted onto above-mentioned PE template (Step II). Later, the microspine coating with hexagonal array consisting of PDMS network was prepared by curing the PDMS precursor at 80 °C for ~2 h and demoulding from the PE template. Finally, the BLOCK was fabricated by immersing the PDMS microspine array into oil bath (e.g., silicone oil) for at least 24 h. Schematic and ESEM images of the microspine coating with hexagonal array before (b, Step III) and after (c, Step IV) oil infusion. All ESEM images from side view are observed at 45° tilt angles. Scale bars, 500 μm (b, c).

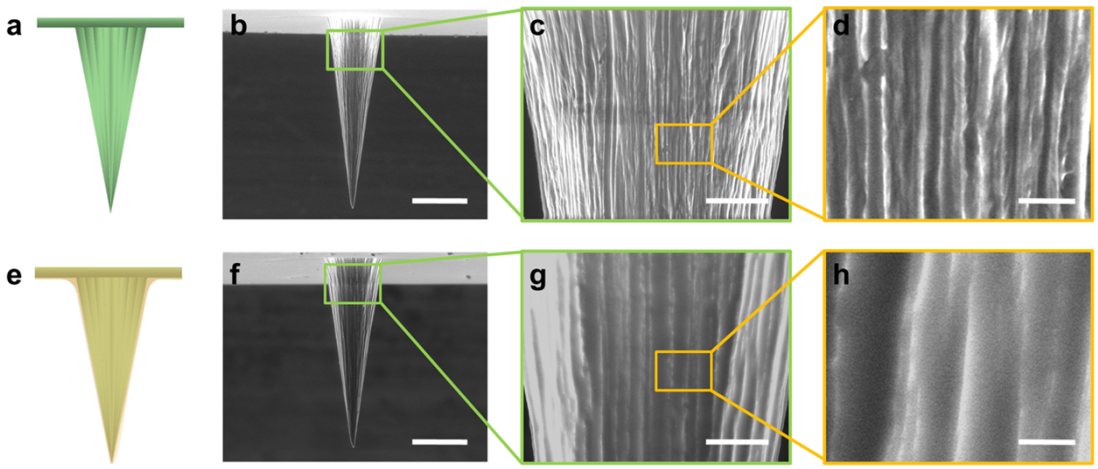

Fig. S3. Surface morphologies of single microspine before and after oil infusion. Schematic of single microspine before (a) and after (e) oil infusion. ESEM and enlarged images in (b-d) and (f-h) represent single microspine before and after oil infusion, respectively. Scale bars, 100 μm (b, f); 25 μm (c, g); 5 μm (d, h).

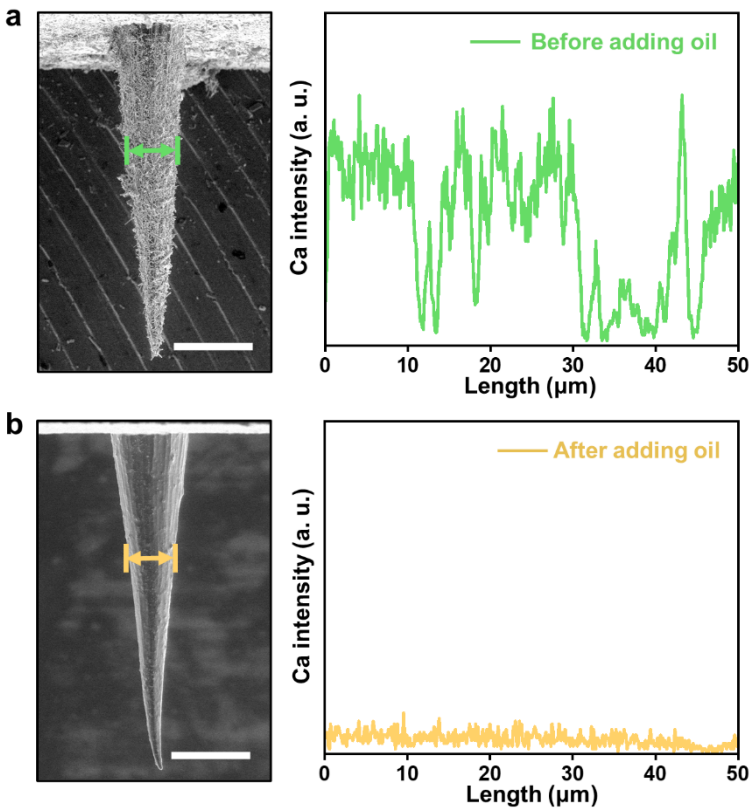

Fig. S4. Completely detachment of scale on single microspine by adding oil. ESEM and corresponding Ca EDS data of the single microspine before (a) and after (b) adding oil. Scale bars: 100 μm.

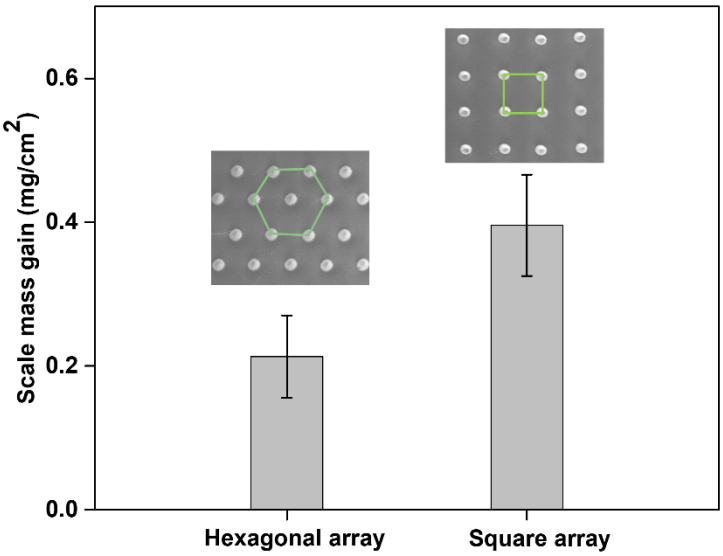

Fig. S5 The influence of microspine array on scale deposition for the BLOCK coating.

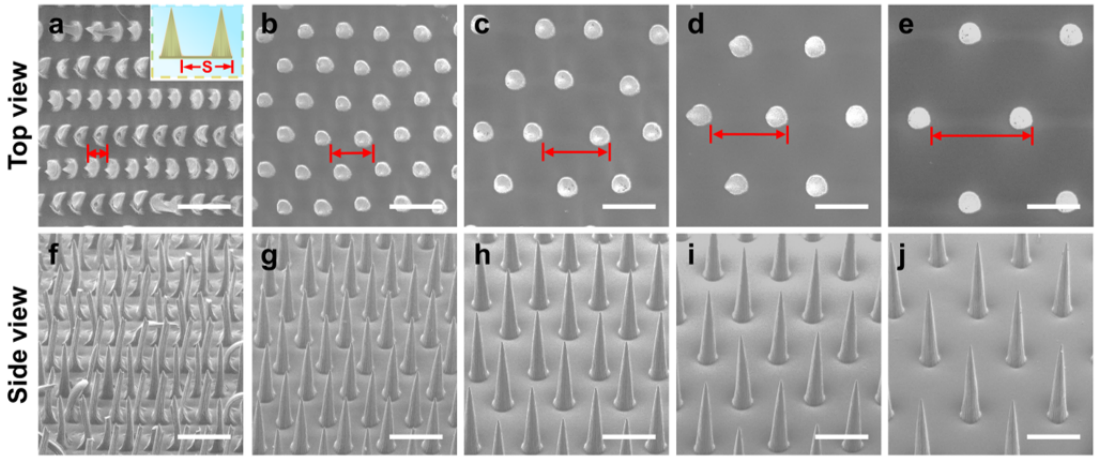

Fig. S6. Surface morphologies of microspine coatings with different microspine spacings. The microspine arrays with the same height (i.e., ca. 500 μm) and different spacings including 205 ± 15 μm (a, f), 382 ± 20 μm (b, g), 601 ± 9 μm (c, h), 782 ± 12 μm (d, i), and 992 ± 11 μm (e, j). All ESEM images from side view are observed at 45° tilt angles. Scale bars: 500 μm.

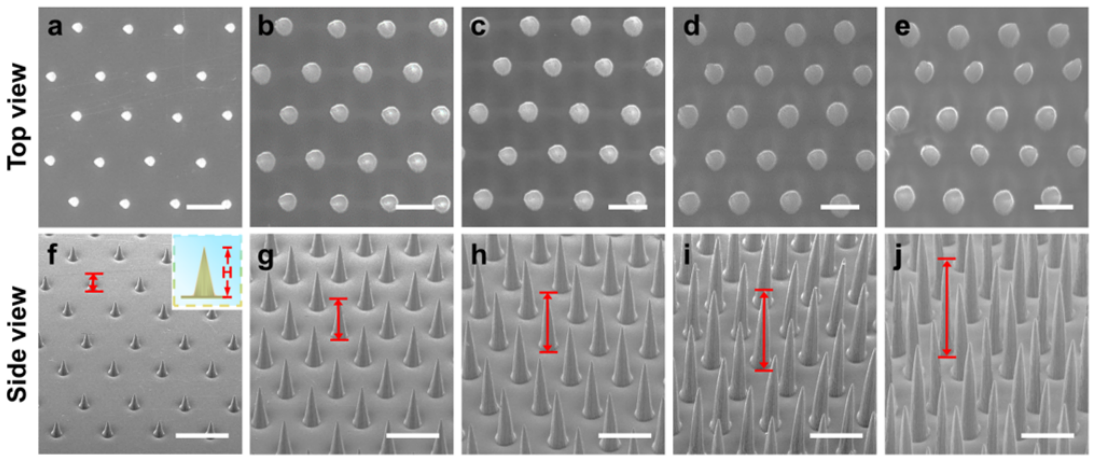

Fig. S7. Surface morphologies of microspine coatings with different microspine heights. The microspine arrays with the same spacing (i.e., ca. 500 μm) and different heights including 232 ± 13 μm (a, f), 531 ± 20 μm (b, g), 765 ± 19 μm (c, h), 1008 ± 11 μm (d, i) and 1243 ± 25 μm (e, j). All ESEM images from side view are observed at 45° tilt angles. Scale bars: 500 μm.

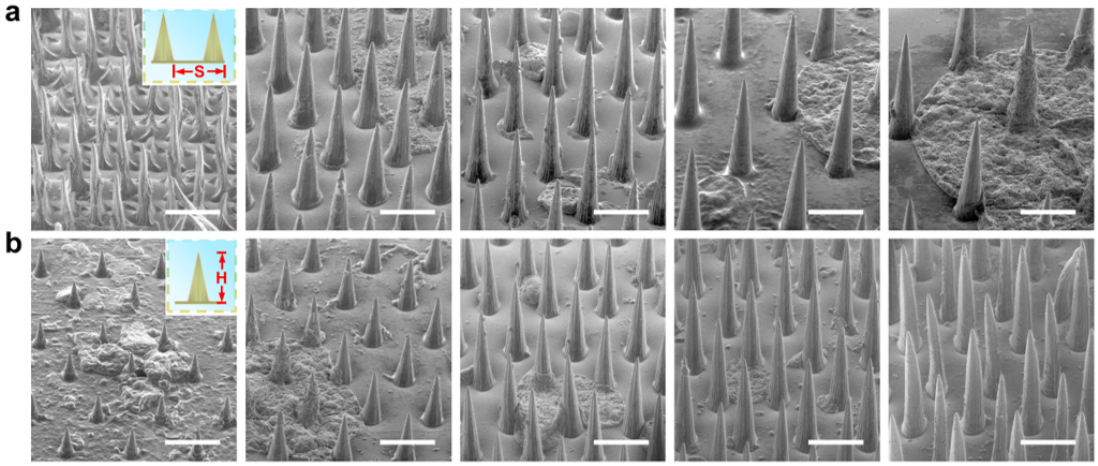

Fig. S8. Influence of microspine spacings and heights on scale deposition. (a) Scale deposition performance on BLOCKs with different spacings (i.e., 205 ± 15 μm, 382 ± 20 μm, 601 ± 9 μm, 782 ± 12 μm and 992 ± 11 μm). (b) Scale deposition performance on BLOCKs with different heights (i.e., 232 ± 13 μm, 531 ± 20 μm, 765 ± 19 μm, 1008 ± 11 μm and 1243 ± 25 μm). All ESEM images from side view are observed at 45° tilt angles. Scale bars: 500 μm.

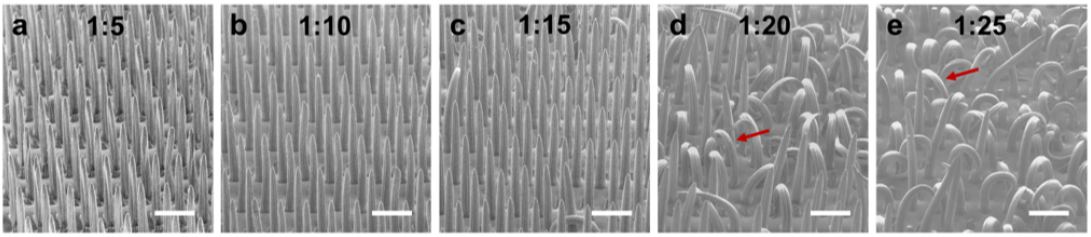

Fig. S9. Surface morphologies of BLOCKs with different crosslinking ratios. ESEM images of BLOCKs with crosslinking ratios of curing agent and silicone oligomer varying from 1:5 to 1:25 (wt/wt). The fallen of microspine is emphasized by red arrows. All ESEM images from side view are observed at 45° tilt angles. Scale bars: 500 μm.

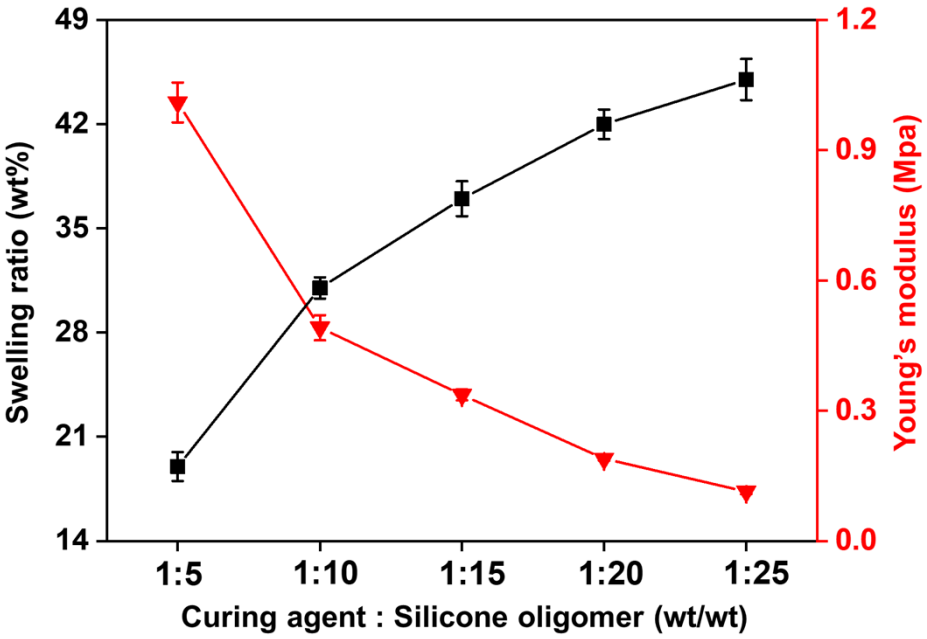

Fig. S10. Effect of crosslinking ratio on swelling ratio and Young's modulus of PDMS. With the crosslinking ratio varying from 1:5 to 1:25 (wt/wt), the swelling ratio of PDMS component gradually increases, while the corresponding Young's modulus always decreases.

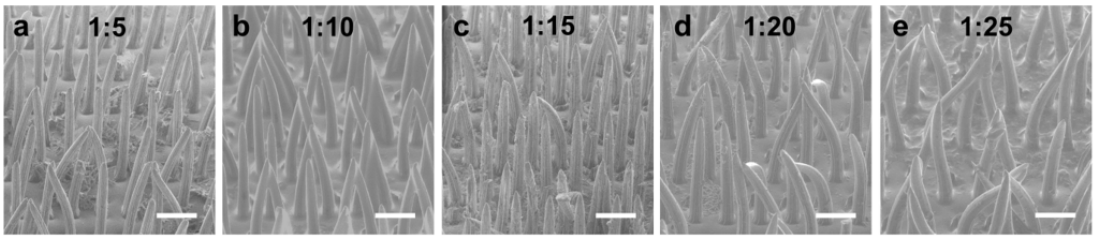

Fig. S11. Scale deposition on BLOCKs with different crosslinking ratios. Scale deposition performance on BLOCKs with the crosslinking ratio of curing agent and silicone oligomer varying from 1:5 to 1:25 (wt/wt). All ESEM images from side view are observed at 45° tilt angles. Scale bars: 200 μm.

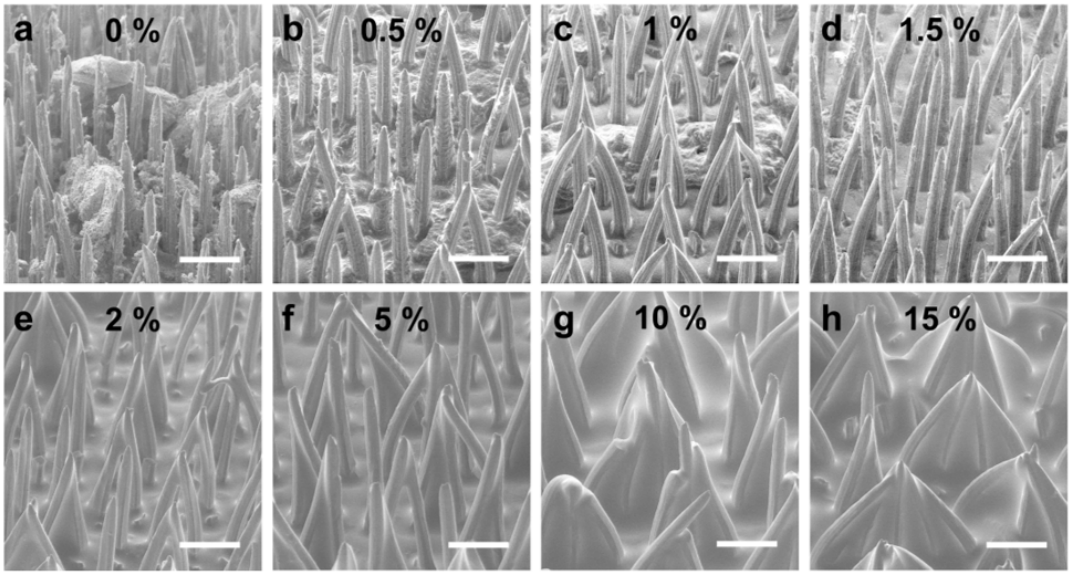

Fig. S12. The influence of oil contents on scale deposition. ESEM images show scale deposition performance on BLOCKs in flowing oil/brine mixtures bearing varied oil contents from 0 to 15%. All ESEM images from side view are observed at 45° tilt angles. Scale bars: 300 μm.

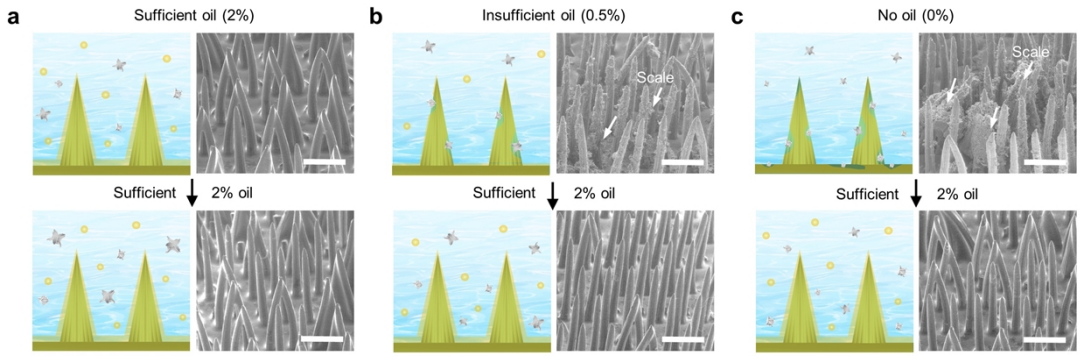

Fig. S13. Three representative situations of oil content in the oil/brine mixture on scale deposition. Schematic and ESEM images of three representative situations for scale deposition in flowing oil/brine mixture. Firstly, the BLOCKs were immersed in sufficient oil (e.g., 2% oil) or insufficient oil (0.5% oil or 0%) for 24 h, followed by extra 24 h immersion in 2% oil. White arrows in (b, c) indicate the scale deposited on the BLOCKs. All ESEM images are viewed at 45° tilt angles. Scale bars, 500 μm.

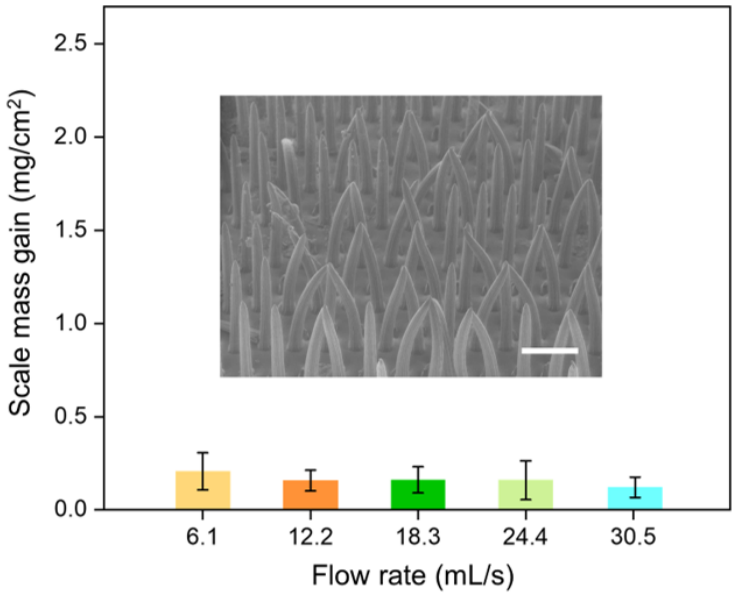

Fig. S14. Scale deposition on BLOCKs with different flow rates. Quantitative analysis of scale deposition on BLOCKs with flow rates varying from 6.1 to 30.5 mL/s with sufficient oil (2%) in the oil/brine mixture. Scale bar: 500 μm.

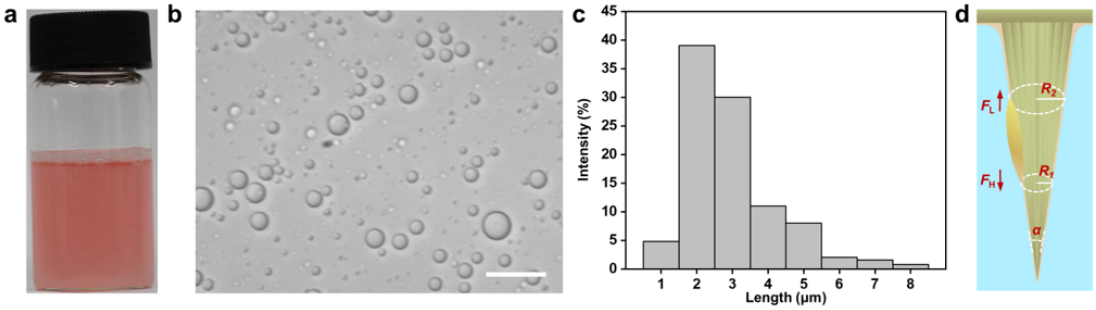

Fig. S15. Characterization of oil microdroplets and schematic of underwater oil collection. (a) By ultrasonically treating and stirring the mixture of oil and brine, an artificial oilfield produced water (e.g., silicone oil, 2% v/v) was prepared. The oil was pre-stained with oil red O. (b) Optical image of the micro-sized oil droplets in the oil/brine mixture. (c) The diameter of oil droplets mainly ranges from 2 to 5 μm. (d) Schematic of underwater collection process of an oil droplet on the oil-infused microspine. Scale bar: 20 μm (b).

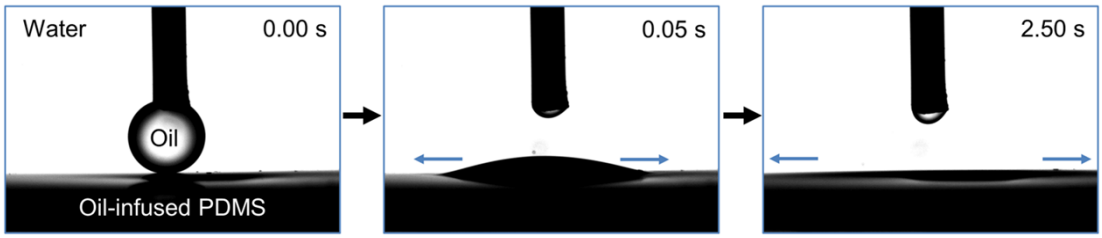

Fig. S16. Spreading of the oil droplet on oil-infused PDMS. In salt solution, an oil droplet rapidly spread on the oil-infused PDMS.

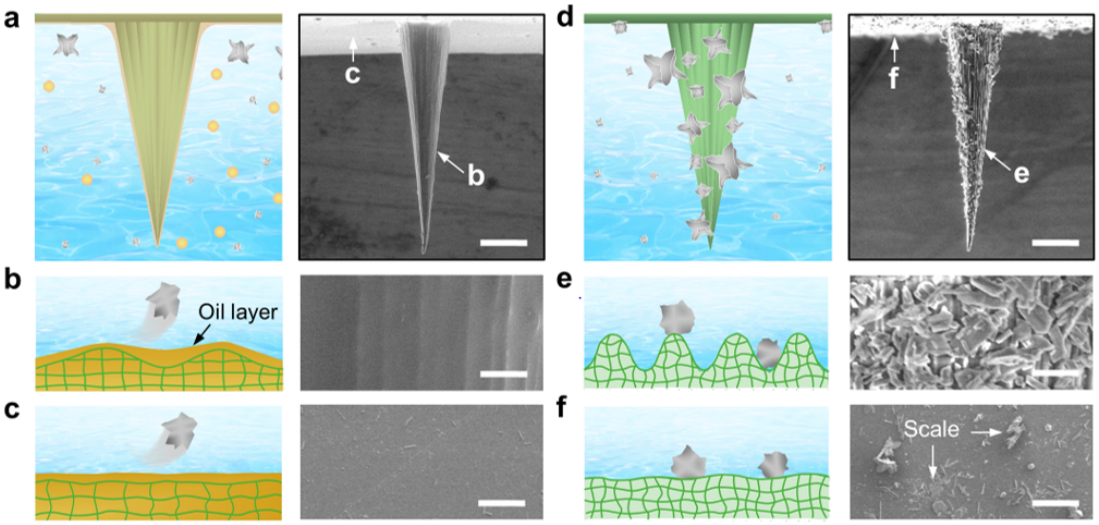

Fig. S17. Scale deposition on a single microspine with/without oil-infusion. (a-c) ESEM image and enlarged images show a single oil-infused microspine after flowing in an oil/brine mixture for ~24 h. (d-f) ESEM image and enlarged images show a single microspine covered with scale after flowing in a pure brine for ~24 h. Scale bars, 200 μm (c, f); 100 μm (a, d); 10 μm (b, e).

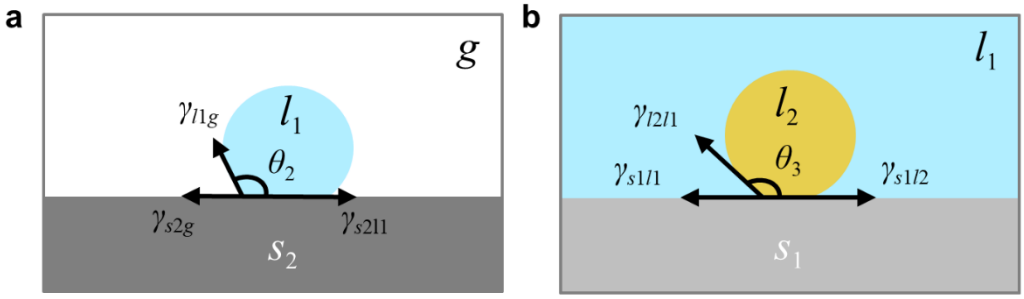

Fig. S18. Scheme of contact angle and interfacial force of specific systems. (a) A salt droplet on the substrate in air. (b) An oil droplet on scale crystal in a salt solution. s_1 and s_2 represent scale crystal and the substrate. l_1 and l_2 are salt solution and oil, respectively. θ_2 is the contact angle of a salt droplet on the substrate in air and θ_3 is the contact angle of oil droplet on scale crystal in a salt solution.

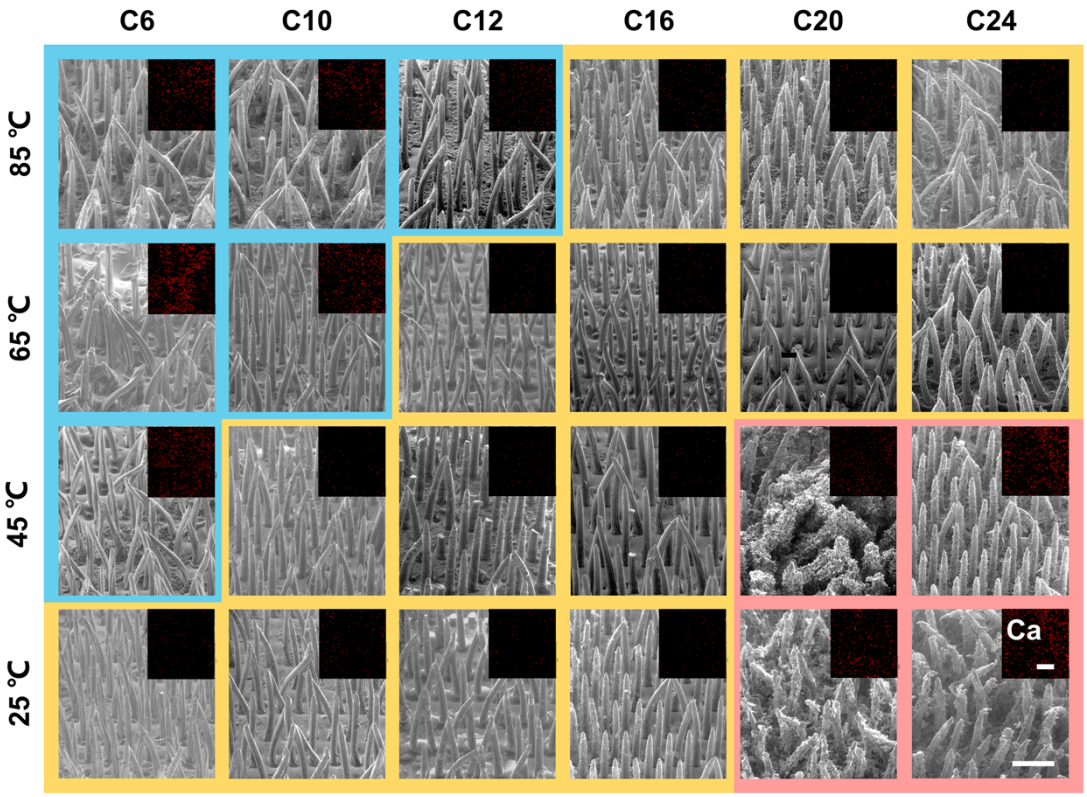

Fig. S19. Effect of oil types and temperatures on scale deposition. Scale deposition performance on BLOCKs bearing oil types from C6 to C24 at the temperature from 25 to 85 °C. The background color represents states of oil layer (blue for volatile state, yellow for liquid state and pink for waxy state). The insets show the corresponding EDS mapping of Ca element. Scale bars: 500 μm; insets, 500 μm.

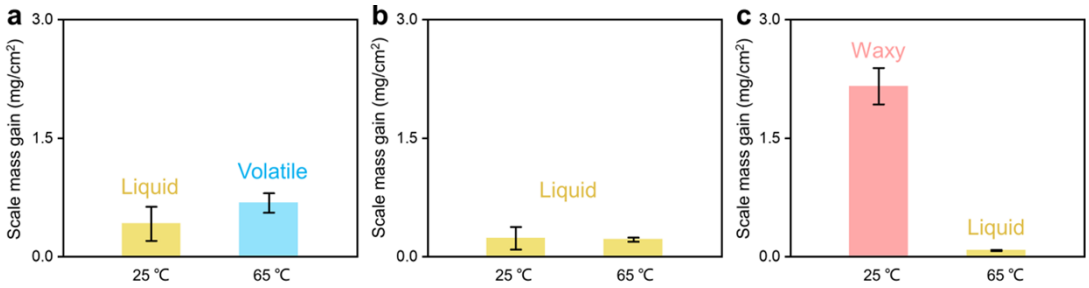

Fig. S20. The effect of temperature on scale deposition by employing oils with distinctive melting and boiling points. (a) For n-alkanes with a lower carbon chain (C6), the SMG value was slightly increased from 0.42 ± 0.22 to 0.68 ± 0.12 mg/cm^2 due to its evaporation-induced depletion when temperature increases from 25 to 65 ℃. (b) For a mediate carbon chain (C16), it always keeps a liquid state between 25 and 65 ℃, thereby achieving an effective scale-resistant capability with a lower SMG value (~0.22 mg/cm^2). (c) When the temperature increases from 25 to 65 ℃, a higher carbon chain (C24) transformed from waxy to liquid state, thereby leading to the significant decrease of the SMG value from 2.16 ± 0.23 to ~0.08 mg/cm^2.

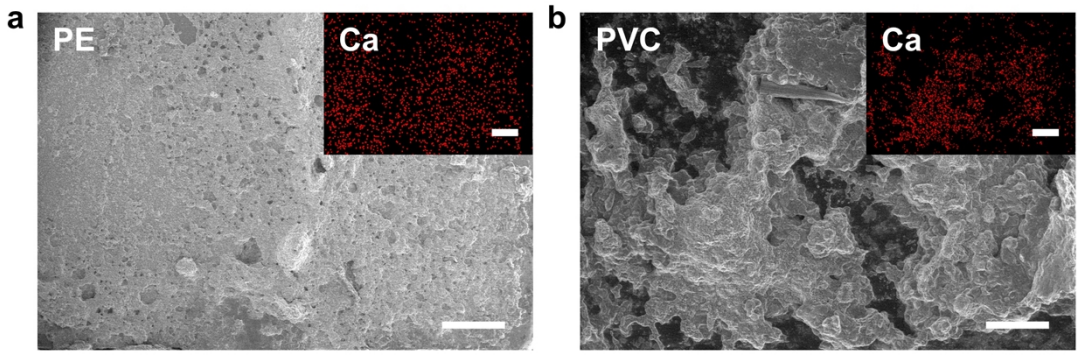

Fig. S21. Scale deposition performance on different substrates. After 35 days immersion in a flowing artificial oilfield produced water (2% oil), ESEM and corresponding Ca mapping images of PE (a) and PVC (b), respectively. Scale bars: 500 μm; insets, 500 μm.

3. Supplementary Tables

Table S1. Interfacial energies between different phases.

Interface	Interfacial energy	Interfacial energy (mJ/m^2)	Data source
Substrate-air	γ_{s2g}	20.7	Reference [2]
Salt solution-air	γ_{l1g}	72.8	Reference [2]
Crystal nucleus-substrate	γ_{s1s2}	10.1	Equation (S6)
Crystal nucleus-salt solution	γ_{s1l1}	95	Reference [11]
Oil-salt solution	γ_{l2l1}	35	Reference [2]
Substrate-salt solution	γ_{s2l1}	44.2	Equation (S5)
Scale crystal-salt solution	γ_{s3l1}	-21	Equation (S11)
Scale crystal-substrate	γ_{s3s2}	12.7	Equation (S11)

Note: s_1, s_2, s_3, l_1, l_2 and g denote crystal nucleus, substrate, scale crystal, salt solution, oil and air, respectively. To avoid the experimental error, we use the surface tension components of water instead of salt solution because the salt solution and water have similar surface tension.[12]

Table S2. Surface energy of the BLOCK, PDMS, water and gypsum. [2, 10, 11]

Material	Surface energy (mJ/m^2)			
	γ	γ^{LW}	γ^+	γ^-
BLOCK	20.7	20.7	0	0
PDMS	20.7	20.7	0	0
Water	72.8	22.6	25.5	25.5
Gypsum	59.7	41.1	1.3	65.5

Note: γ denotes surface tension. γ^{LW} is the Lifshitz−van der Waals component of surface energy. γ^+ and γ^- are the polar components from the Lewis acid and Lewis base sites, respectively.

Table S3. Melting and boiling points of various oil types.[2, 13]

Oil type	Melting point (°C)	Boiling point (°C)
C6	-95.3	68.7
C10	-29.7	174.1
C12	-9.6	216.3
C16	18.2	287
C20	36-38	343
C24	45-52	351
Silicone oil (10 cSt)	-59	101

4. Supplementary Movies

Movie S1: Oil collection on oil-infused single microspine. An oil droplet moved quickly from tip to bottom of the microspine in an artificial oilfield produced water. As a result, the oil droplet could be continuously collected from the oil/brine mixture.

Movie S2: High temperature de-scaling for a large-scale BLOCK infused by waxy oil. After scaling in brine at 25 °C for ca. 3 days, massive scales were observed on a large-scale BLOCK (20 cm × 20 cm) infused by waxy oil (C24). The deposited scale was easily removed after immersing in 65 ℃ water for ca. 2 min.

References

1 K. Li, J. Ju, Z. Xue, J. Ma, L. Feng, S. Gao and L. Jiang. *Nat. Commun.* **2013**, *4*, 2276.
2 S. Peppou-Chapman, J. K. Hong, A. Waterhouse and C. Neto. *Chem. Soc. Rev.* **2020**, *49*, 3688-3715.
3 X. Chen, G. Wen and Z. Guo. *Mater. Horiz.* **2020**, *7*, 1697-1726.
4 P. Zhang, F. Zhang, C. Zhao, S. Wang, M. Liu and L. Jiang. *Angew. Chem. Int. Ed.* **2016**, *55*, 3615-3619.
5 K. C. Russell. *Adv. Colloid Interf. Sci.* **1980**, *13*, 205-318.
6 N. H. Fletcher. *J. Chem. Phys.* **1958**, *29*, 572-576.
7 J. Restolho, J. L. Mata and B. Saramago. *J. Colloid Interf. Sci.* **2009**, *340*, 82-86.
8 C. J. Van Oss, R. J. Good and M. K. Chaudhury. *Langmuir* **1988**, *4*, 884-891.
9 C. J. Van Oss, M. K. Chaudhury and R. J. Good. *Chem. Rev.* **1988**, *88*, 927-941.
10 R. Zhang and G. Azimi. *ACS Appl. Mater. Interfaces* **2020**, *12*, 42339-42347.
11 A. Masoudi, P. Irajizad, N. Farokhnia, V. Kashyap and H. Ghasemi. *ACS Appl. Mater. Interfaces* **2017**, *9*, 21025-21033.
12 J. M. Rimsza and K. L. Kuhlman. *Langmuir* **2020**, *36*, 2482-2491.
13 K. A. Kobe and R. E. Lynn. *Chem. Rev.* **1953**, *52*, 117-236.